Anisotropic magnetization of the III-VI diluted magnetic semiconductor $In_{1-x}Mn_xS$ in the mixed state

J. L. Tracy, G. Franzese, Ashlee Byrd, J. Garner, and T. M. Pekarek
Department of Chemistry and Physics, University of North Florida, Jacksonville, Florida 32224, USA

I. Miotkowski and A. K. Ramdas
Department of Physics, Purdue University, West Lafayette, Indiana, USA
(Received 31 May 2005; revised manuscript received 15 August 2005; published 6 October 2005)

The anisotropic magnetization of the III-VI diluted magnetic semiconductor (DMS), $In_{1-x}Mn_xS$, is found within a mixed state model and compared to our measurements. The compound has a markedly different crystal structure from previously investigated III-VI DMS crystals. The singlet portion of the Hamiltonian incorporates the interaction of the incomplete shell of Mn $3d$ electrons with the crystal lattice within the point-ion approximation. Other terms include the Zeeman, spin-orbit and the spin-spin interactions. The doublet portion of the Hamiltonian assumes the substitutional nearest-neighbor Mn atoms interact with each other via antiferromagnet superexchange coupling. For our samples, the nominal value of $x=2\%$. The singlet magnetization is found from the energy eigenvalues of the singlet Hamiltonian matrix, which was expressed in terms of an uncoupled angular momentum basis set. Magnetization versus temperature and field results are found for several values of the magnetic field, **B**, including choices along various directions relative to the underlying lattice. The magnetization was measured over a wide range of temperatures and fields with results compared to the mixed state model, which is an average of the singlet and doublet magnetizations. Overall, the agreement of the theory with the experimental data is excellent except at low temperatures ($<\approx 10$ K) where some evidence of possible spin-glass behavior is evident.

DOI: 10.1103/PhysRevB.72.165201 PACS number(s): 75.50.Pp, 75.10.Dg, 75.60.Ej, 75.20.−g

I. INTRODUCTION

In recent years a number of papers have focused on the electronic structure[1,2] and the transition metal interactions[3–5] in III-V diluted magnetic semiconductor (DMS) systems where the magnetization arises due to the doping of the semiconducting host with transition metal atoms. Noteworthy in this regard are the numerous investigations of $Ga_{1-x}Mn_xAs$ where in some studies evidence or predictions of ferromagnetic behavior have been reported.[6–8] Evidence of ferromagnetism[9] and investigations of the electronic structure[10,11] of II-VI DMS systems have also seen intense work during the past several years. These materials are of practical interest because of their potential for use in laser devices or possible utility in spintronic applications.

Another class of DMS systems has received less attention, the III-VI DMS materials. The III-VI DMS class of compounds offer alternative materials and crystal structures to the III-V and II-VI DMS systems and therefore may also be useful in the laser and spintronic applications alluded to above. The first III-VI DMS system to be investigated was $Ga_{1-x}Mn_xS$ where the magnetization was measured with excellent agreement between theory and experiment.[12] This new class of DMS crystals is prepared by adding trace amounts of manganese to the III-VI semiconducting host. It is assumed the transition metal atoms enter the crystal by substituting randomly for some of the group III atoms and give rise to the magnetization found in the samples. To date, measurements of the magnetization have been performed on the following set of III-VI DMS compounds[13–16]: $Ga_{1-x}Mn_xSe$, $Ga_{1-x}Mn_xS$, and $Ga_{1-x}Fe_xSe$. A number of promising electro-optical applications have been proposed for these doped[17,18] and undoped[19–22] (GaSe and InSe) materials due to their nonlinear optical properties. The III-VI DMS materials represent a relatively unexplored class of materials especially from a theoretical standpoint. This paper presents a model of only the second III-VI DMS compound for which a successful model of the magnetization has been found.

We present a model and measurement of the magnetization of $In_{1-x}Mn_xS$, a member of the III-VI DMS class that has a markedly different crystal structure from previously studied systems.[23] The findings cover a wide range of temperatures and applied magnetic fields. The computed magnetization was found for applied fields with several orientations relative to the underlying lattice including parallel and perpendicular directions relative to the c axis. The calculated magnetization exhibited significant anisotropy and for these two extreme field directions the computed magnetization generally was found to bracket the measured magnetization. By suitable angular averaging, which is justified based on the crystal structure detailed below, the agreement between experiment and model magnetization is excellent.[24]

Additional measurements (e.g., optical absorption) would be advantageous in order to more accurately determine the crystal field parameters used in the model. Indeed, more accurate parameters should help somewhat to extend the domain of agreement of theory and measurement. Moreover, an extension of the model beyond the standard point-ion approximation to include the influence of the covalent bonds on the crystal potential would be a helpful enhancement to the model. However, this may be difficult to accomplish.[25]

II. CRYSTAL STRUCTURE AND TRANSITION METAL HAMILTONIAN

A. The singlet model

In order to determine the magnetization of this compound we begin by finding the $3d$-electron energy levels of the transition metal atom (Mn) placed in the III-VI crystal (InS) in the presence of an applied magnetic field, **B**. We assume the Mn atoms randomly substitute for a fraction of the group III atoms and the Mn is bonded to the four nearest-neighbor atoms via covalent bonds.[26] The incomplete $3d$ valence shell of the Mn gives rise to the magnetic moment of the sample. The energy levels of the $3d$ electrons of the Mn atom are perturbed by the crystal field produced by its neighbors; here we consider only nearest-neighbor interactions. Within the point-ion approximation, which is the standard model in DMS calculations, the covalent bonds are replaced by ionic bonds between point ions having formal oxidation states we denote Z (for S) and Z' (for In). The energy levels are then determined by, among other variables, the crystal symmetry, distance between ions, bond angles, and the values chosen for Z and Z'. Such bonding properties must be determined from experiment. The bond lengths (denoted R for Mn-S and R' for Mn-In) have been measured[27] for a similar material, GaSe, and these values were used for the InS studied here. Note, since $R' \neq R$, the system does not have pure tetrahedral symmetry although we will assume the bond angles are the same as in a tetrahedron. Our results were not very sensitive to bond lengths and consequently, using the GaSe data should not introduce significant error.

The orthorhombic crystal structure of InS is shown[23] in Fig. 1. The manganese ion resides at the center of the elongated tetrahedron with three Mn-S covalent bonds ($R \cong 2.473$ Å in GaSe) and one Mn-In covalent bond ($R' \cong 2.388$ Å in GaSe). The angle between the Mn-In bond and each of the Mn-S bonds was assumed to be $\theta = 109.5°$. Throughout one-half the crystal the Mn-In bonds have one orientation (say 0°) while over the other one-half the Mn-In bonds make an angle of 70.53° with respect to the first set of Mn-In bonds. As discussed above, the Mn-S and Mn-In covalent bonds are replaced by ionic bonds with the sulfur atoms in the formal oxidation state $Z=-2$ and the indium atoms in formal oxidation state $Z'=+2$. As in the prior III-VI DMS studied ($Ga_{1-x}Mn_xS$) here we expect the Mn to exist in the +3 formal oxidation state.[12] The Mn^{+3} has a $3d^4$ outer electron configuration and a ^5D ground state term according to Hund's rules. The crystal field should exert a strong influence on the $3d$ energy levels of the Mn^{+3} ion.

Within the singlet model of noninteracting Mn ions the Hamiltonian for an isolated transition metal ion in the semiconducting crystal host has the well-known form[28]

$$H_{\text{singlet}} = H_{\text{free-ion}} + H_{\text{crystal}} + H_{\text{spin-orbit}} + H_{\text{spin-spin}} + H_{\text{Zeeman}}, \tag{1}$$

where $H_{\text{free-ion}}$ is the Hamiltonian of the free ion [for the $3d^4$ Mn ion $(2L+1)(2S+1)=25$-fold degenerate ground term, ^5D], the spin-orbit Hamiltonian,

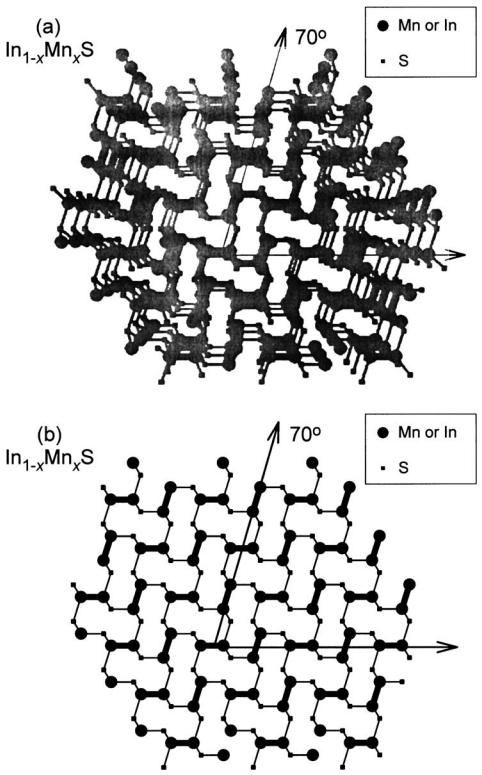

FIG. 1. The orthorhombic crystal structure of InS (cf. Ref. 8).

$$H_{\text{spin-orbit}} = \lambda \mathbf{L} \cdot \mathbf{S}, \tag{2}$$

the spin-spin Hamiltonian,

$$H_{\text{spin-spin}} = -\rho\left[(\mathbf{L}\cdot\mathbf{S})^2 + \tfrac{1}{2}(\mathbf{L}\cdot\mathbf{S}) - \tfrac{1}{3}L(L+1)S(S+1)\right], \tag{3}$$

and the Zeeman Hamiltonian,

$$H_{\text{Zeeman}} = \mu_B(\mathbf{L} + 2\mathbf{S})\cdot\mathbf{B}. \tag{4}$$

In the above equations, $\mathbf{L}(\mathbf{S})$ is the total orbital (spin) operator for the d electrons of the transition metal ion, **B** the applied magnetic field, μ_B the Bohr magneton, and $L(S)$ the total orbital (spin) quantum numbers ($L=S=2$, for the ground term).

The crystal field term of the Hamiltonian in Eq. (1) is found by expanding in spherical harmonics the Coulomb potential for the interaction of the Mn d electrons with the ionic nuclei. The electron positions, $\{\mathbf{r}_i\}$ $(i=1,2,3,4)$, and the nearest-neighbor crystal point-ion positions of the nuclei we denote, $\{\mathbf{R}_j\}$ $(j=1,2,3,4)$, which appear in the expression below,

$$H_{\text{crystal}}(\{\mathbf{r}_i\},\{\mathbf{R}_j\}) = -e\sum_i \sum_j \frac{eZ_j}{|\mathbf{R}_j - \mathbf{r}_i|} = \sum_i \sum_l \sum_{m=-l}^{l} A_l^m r_i^l Y_l^m(\theta_i,\phi_i), \tag{5}$$

where

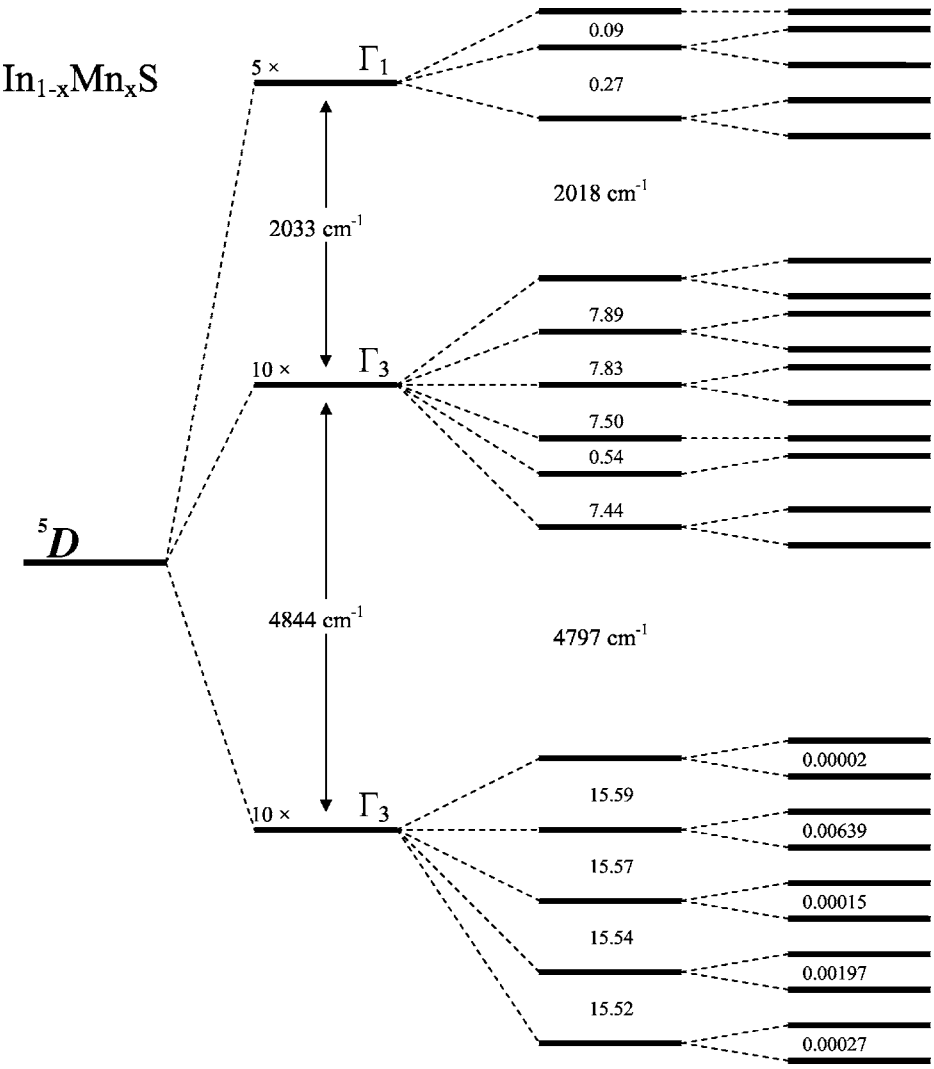

FIG. 2. The energy level diagram for the d electrons of the Mn^{+3} within the InS crystal. The splitting of the levels due to crystal field, spin-orbit, and spin-spin terms of the Hamiltonian is featured. There are a total of 25 states. The energies are in units of cm^{-1}.

$$H_{\text{free-ion}} + H_{\text{crystal}} + H_{\text{spin-orbit}} + H_{\text{spin-spin}}$$

$$A_l^m \equiv \frac{4\pi e^2}{2l+1} \sum_j \frac{Z_j Y_l^{m*}(\theta_j, \phi_j)}{R_j^{l+1}}.$$

In most instances optical absorption data are used to determine the energy level splitting by the crystal field (see Ref. 28, p. 394) because of the errors introduced by the point-ion approximation used in Eq. (5). In the absence of optical data for $In_{1-x}Mn_xS$, we have used the crystal field levels based on Eq. (5) with values of Z and Z' quoted above. One would expect the covalent bonds present in the crystal to introduce shielding effects which would suggest using different values for Z and Z' than the above "bare" (unshielded) values that we have used. Rather than adjusting the values of Z and Z', we have instead used the spin-orbit coupling constant, λ, as a fitting parameter. Therefore, in the $In_{1-x}Mn_xS$ results presented below, we used $\rho=0.18\ cm^{-1}$ (see Ref. 28) and $\lambda = 7.8\ cm^{-1}$, a value of λ somewhat smaller than the value used in the $Ga_{1-x}Mn_xS$ system, and even smaller yet than the free-ion value quoted in Ref. 28. It has long been known that

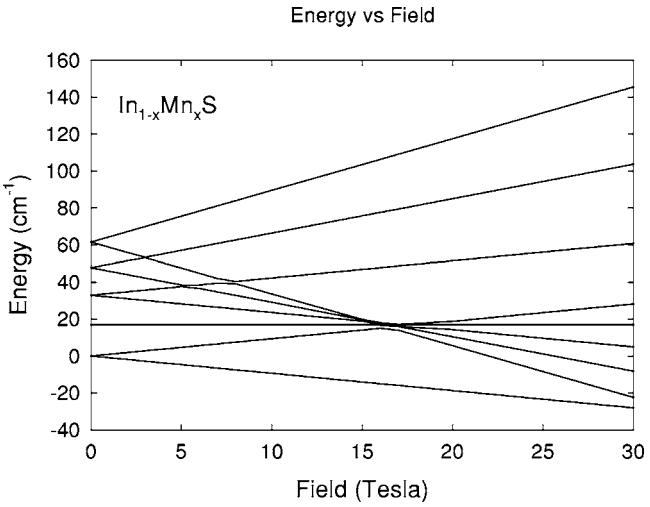

FIG. 3. Energy (cm^{-1}) versus field (Tesla) for the 10 lowest energy states of Fig. 2.

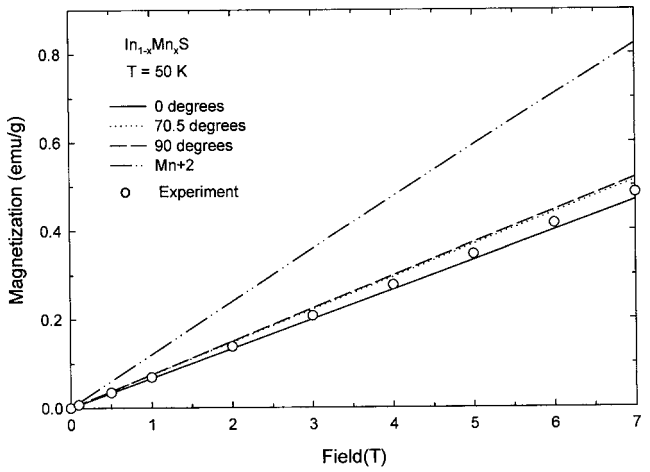

FIG. 4. Magnetization (emu/g) versus field up to 7 Tesla for temperature $T=50$ K. The open circles represent the experimental data. The Mn^{+3} singlet model theory assumes the following angles for the magnetic field, $\theta_B=0°$, 70.5°, and 90°. Notice the bracketing of the experimental data by the 0° and 90° theory curves. The top curve assumes the oxidation state, Mn^{+2}, which represents the magnetization in terms of the Brillouin function.

λ may be significantly reduced from its free-ion value when the ion is placed in a crystal.

Due to the crystal symmetry (point group symmetry C_{3v} at the transition metal site) only the following A_l^m's are nonzero: $A_2{}^0, A_4{}^0, A_4{}^3 = -A_4{}^{-3}$. The operator equivalent crystal field Hamiltonian[12,29,30] we find to be

$$H_{\text{crystal}} = b[3L_z{}^2 - L(L+1)] + a\{35L_z{}^4 + [25 - 30L(L+1)]L_z{}^2 + 3L^2(L+1)^2 - 6L(L+1)\} - d\{L_z, L_+{}^3 + L_-{}^3\}. \quad (6)$$

Here $L_\pm \equiv L_x \pm i\, L_y$ and L_x, L_y, and L_z are the components of the total orbital angular momentum operator along the Cartesian axes, **x**, **y**, and **z**. In Eq. (6), { } represents an anticommutator and the coefficients are given by

$$b \equiv A_2^0 \langle\alpha\rangle \langle r^2\rangle \sqrt{5/16\pi},$$

$$a \equiv A_4^0 \langle\beta\rangle \langle r^4\rangle \sqrt{9/256\pi},$$

$$d \equiv A_4^3 \langle\beta\rangle \langle r^4\rangle \sqrt{1.23/\pi},$$

where for Mn^{+3} (Ref. 28), $\langle\alpha\rangle = 2/21$, $\langle\beta\rangle = -2/63$, $\langle r^2\rangle = 1.286$ a.u. (atomic units), and $\langle r^4\rangle = 3.466$ a.u.

A matrix representation of the Hamiltonian was obtained using the "uncoupled" angular momentum basis states, $|LSM_LM_S\rangle$. In the case of Mn with $3d^4$, $L=S=2$ and both M_L and $M_S = 0, \pm 1, \pm 2$. The full Hamiltonian matrix has dimensions 25×25. The diagonalization of the Hamiltonian was performed numerically.

The singlet model energy level diagram is shown in Fig. 2. The crystal field interaction splits the degenerate free ion term into an orbital set of levels having two orbital doublets and a higher energy orbital singlet. Since the spin-orbit interaction incorporates the intrinsic spin of the electrons this further splits some of the orbital degeneracies. The spin-spin term further splits the states by a small amount (<0.01 cm^{-1}), lifting all remaining degeneracies for a total of 25 states available for the *d* electrons.

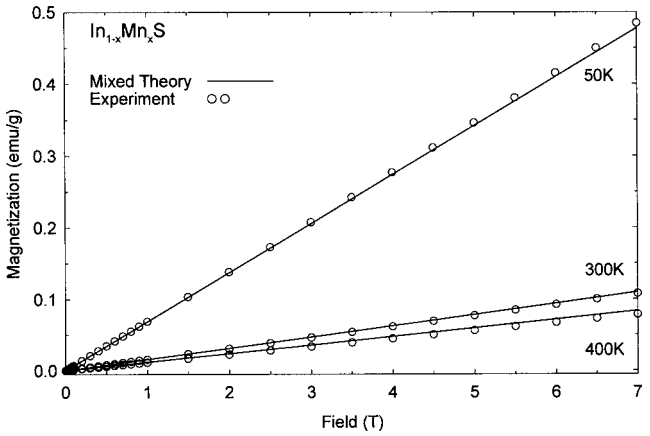

FIG. 5. Magnetization (emu/g) versus field up to 7 Tesla and for three fixed temperatures, 50, 300, and 400 K. The mixed model results are angular averages using 0° and 70.53° for the applied field directions. The agreement of the model with the experimental data (circles) is excellent over this wide range of parameter space.

Normally the lowest energy levels in Fig. 2 are the levels responsible for the magnetization properties of experimental samples. Shown in Fig. 3 is the dependence of the 10 lowest energy states on the applied magnetic field. As we shall see below, the magnetization depends on the energy and the slopes of the energy states versus field.

B. The doublet model

The singlet model neglects interactions between the transition metal atoms. In this paper we extend the singlet model to the doublet model that incorporates the interaction between nearest-neighbor transition metal atoms. In the results

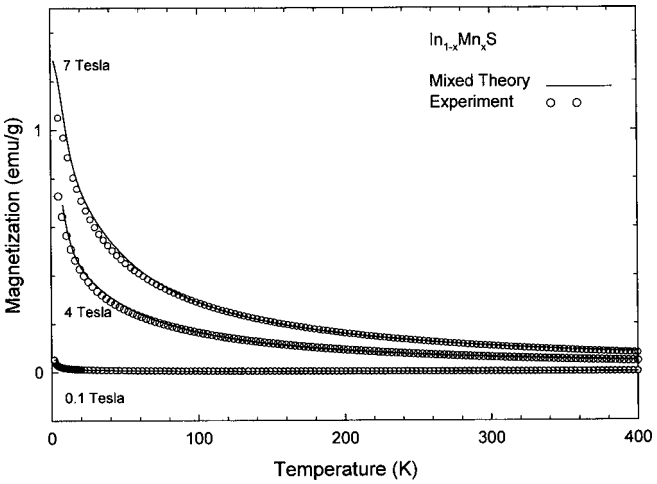

FIG. 6. Magnetization (emu/g) versus temperature up to 400 K and for three fixed fields, 0.1, 4, and 7 Tesla. The mixed model results are angular averages using 0° and 70.53° for the applied field directions. The agreement of the model with the experimental data (circles) is excellent over this wide range of parameter space.

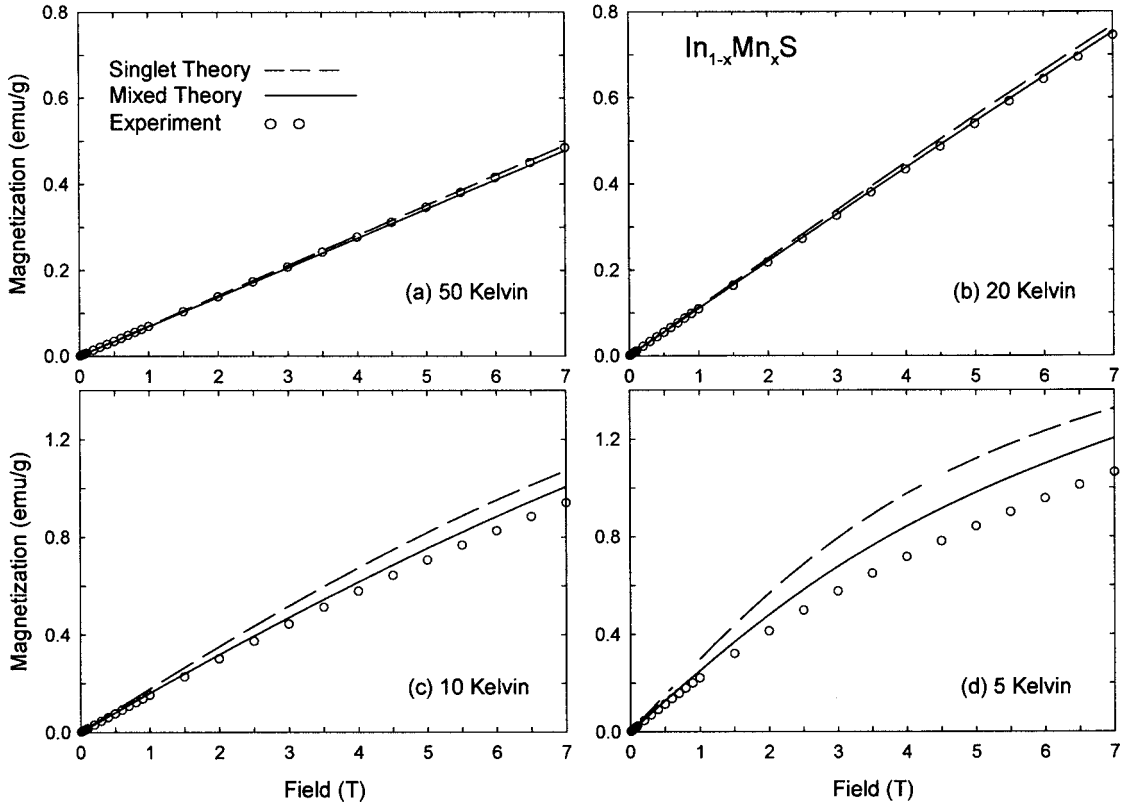

FIG. 7. Magnetization (emu/g) versus field (Tesla) for four fixed temperatures, (a) 50, (b) 20, (c) 10, and (d) 5 K. The circles represent the measured magnetization, while the other two curves are angular averages of magnetization using 0° and 70.53° for the applied field directions and for singlet and mixed models as described in the text.

presented below, we find the computed singlet magnetization is larger than that measured in the laboratory. In the doublet model, therefore, we assume the Mn—Mn coupling to be antiferromagnetic, which lowers the computed magnetization.

If we write the total angular momentum operator for the Mn $3d$-shell electrons as, $\mathbf{J}$, then the doublet Hamiltonian is of the Heisenberg form, and including the effects of an external magnetic field, $\mathbf{B}$, the Hamiltonian takes the form

$$H_{\text{doublet}} = -J_{\text{eff}}\mathbf{J_1}\cdot\mathbf{J_2} + g\mu_B B(\mathbf{J_1}+\mathbf{J_2})\cdot\mathbf{B}. \tag{7}$$

The g in Eq. (7) is 2 and μ_B is the Bohr magneton. For antiferromagnetic coupling the sign of the exchange coupling constant, J_{eff}, is negative. The eigenvalues of H_{doublet} are most easily determined by defining a new total angular momentum operator for the pair, $\mathbf{J_T}=\mathbf{J_1}+\mathbf{J_2}$. The following relations hold[31]: $J_T=J_1+J_2,\ldots,|J_1-J_2|$ and for $\mathbf{B}$ along the z axis with a given value of $J_T, J_{Tz}=J_T\cdots-J_T$. The energy eigenvalues of the doublet Hamiltonian are

$$E_{\text{doublet}} = -J_{\text{eff}}J_T(J_T+1)/2 + g\mu_B B J_{Tz}. \tag{8}$$

In this paper we used $J_1=J_2=4$ and with this choice found the best fit for the value of $J_{\text{eff}}=-6$ K.

C. Magnetization

A given singlet energy level E_i contributes a magnetic moment given by the slope of the energy level versus magnetic field curve, weighted by the Boltzmann factor. The singlet magnetization is found from

$$M(T,B) = -\frac{n(x)}{Z}\sum_{i=1}^{N} e^{-\beta E_i}\frac{\partial E_i}{\partial B}. \tag{9}$$

In Eq. (9), $\beta=1/k_BT$ (with k_B the Boltzmann constant), Z is the partition function,

$$Z(T,B) = \sum_{i=1}^{N} e^{-\beta E_i}, \tag{10}$$

where N is the number of energy levels ($N=25$ for Mn with $3d^4$) and $n(x)$ gives the number of Mn ions per unit mass of the sample for concentration x,

$$n(x) = xN_A/[(1-x)M_{\text{In}} + xM_{\text{Mn}} + M_{\text{S}}], \tag{11}$$

where M_i is the atomic mass of the ith element and N_A is Avogadro's number. Equation (9) is also used to find the doublet magnetization except the energy levels, E_i, are given by E_{doublet} from Eq. (8) and the result must be divided by 2 to avoid double counting a Mn moment.

The mixed state pertains to situations where every Mn atom is either a singlet or a doublet. Using p to denote the probability a Mn atom is a singlet, the average magnetization in the "mixed state" follows:

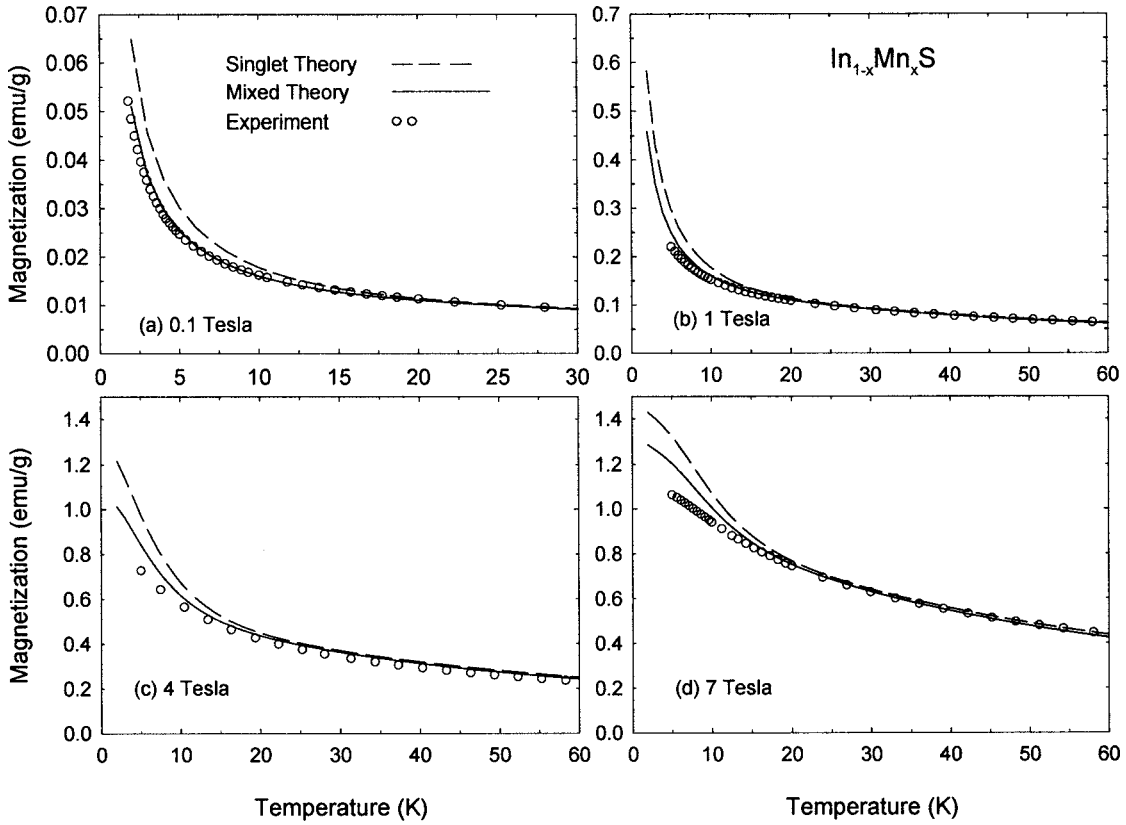

FIG. 8. Magnetization (emu/g) versus temperature (K) for four fixed fields, (a) 0.1, (b) 1, (c) 4, and (d) 7 Tesla. The circles represent the measured magnetization, while the other two curves are angular averages of magnetization using 0° and 70.53° for the applied field directions and for singlet and mixed models as described in the text.

$$M_{\text{mixed}} = pM_{\text{singlet}} + (1-p)M_{\text{doublet}}. \tag{12}$$

For a random substitution of Mn for In atoms, p is found using the expression[13]

$$p = (1-x)^{13}, \tag{13}$$

where x is the concentration of Mn.

III. COMPARISON TO EXPERIMENT

Bulk single-crystalline $In_{1-x}Mn_xS$ samples were taken from boules with nominal concentration $x=2\%$. The sample was grown by the vertical Bridgman method and had a mass of 57.4 mg. Magnetic measurements were made between 1.8 and 400 K in fields up to 7 T using a quantum design MPMS XL7-superconducting quantum interference device (SQUID) magnetometer. The diamagnetic susceptibility of a pure InS crystal was measured to be -3×10^{-7} emu/g G. This contribution to the magnetization due to InS has been subtracted from the data.

The 2% nominal concentration of Mn was the value of x used in the model. As a preliminary step, we first calculated the magnetization versus field (up to 7 Tesla) at several constant temperatures and the magnetization versus temperature (up to 400 K) at several constant fields. This was carried out for two orientations of the applied magnetic field ($\theta_B=0°$, i.e., parallel to the crystal's c axis and at 90°, perpendicular). The results were found to bracket the experimental data. Some of these results for the anisotropic magnetization are illustrated in Fig. 4 for the case $T=50$ K. The top curve in the figure gives the magnetization assuming the Mn ion to be in the +2 formal oxidation state. As was found[12] in the related compound, $Ga_{1-x}Mn_xS$, the magnetization found assuming Mn^{+2} is a Brillouin function that leads to results far above the experimental data and the other Mn^{+3} theory curves in the figure. The experimental data is represented in the figure with the "o." To further illustrate the magnetization anisotropy we have included in Fig. 4 a magnetization curve assuming $\theta_B=70.53°$; the reason for choosing this particular angle will now be addressed.

From the reported crystal structure,[23] one-half of the InMn bonds are aligned along the c axis while the other one-half make an angle of 70.53° with the c axis. This is illustrated in Fig. 1. Another, equally probable scenario has one-half the InMn bonds at 90° to the c axis and the other one-half at 160.53°. Experimentally the crystal alignment would suggest either of these two choices. Consequently in our calculations below we have averaged the magnetization over angles assuming both possible scenarios (i.e., $[M(0°)+M(70.53°)]/2$ and $[M(90°)+M(160.53°)]/2$). In both cases the results were found to be nearly the same. In Figs. 5–8 our model and measurement results are reported. The theory assumes the oxidation state of the Mn to be +3 since the +2 state led to theoretical results that were far above the data, as was discussed earlier. Shown is a plot of the magne-

tization vesus field (Fig. 5) and temperature (Fig. 6) over a wide region of parameter space. One can see the excellent agreement of the mixed model with the experiment from 50 K to 400 K in fields up to 7 Tesla. Figure 7 gives the magnetization versus field (up to 7 Tesla) at the following low temperatures: 50, 20, 10, and 5 K. The figure shows three magnetization curves, the singlet model, "mixed" model, and the experimental data. The agreement between model and experiment is generally excellent but falls off somewhat at the lowest temperatures (<10 K). Clearly, the inclusion of doublets brings the model closer to experiment when compared to singlets alone. In Fig. 8 is shown the magnetization versus temperature at the following applied fields: 0.1, 1, 4, and 7 Tesla. The agreement is once again excellent except at temperatures below about 10 K in a field >1 Tesla.

IV. DISCUSSION AND CONCLUSION

We have measured and modeled the magnetization of the III-VI DMS, $In_{1-x}Mn_xS$, going beyond the singlet model. In all cases considered here the theoretical magnetization found within the singlet model overestimates the magnetization compared to the measured magnetization. By introducing Mn pairs with antiferromagnetic coupling, the angular averaged magnetization calculations agree with the experimental data at temperatures between 50 and 400 K in fields up to 7 T. Agreement between the theory and experimental data begins to deviate only at lower temperatures (<10 K), as expected, as longer range interactions become more significant. Similar disagreement at low temperatures was observed in the II-VI DMS as well as in $Ga_{1-x}Mn_xS$. In the II-VI DMS, the longer range interactions commonly resulted in a transition to the spin-glass state.[32]

$In_{1-x}Mn_xS$ has a crystal structure that differs substantially from the only other III-VI DMS structure previously modeled,[12] $Ga_{1-x}Mn_xS$. In the simpler $Ga_{1-x}Mn_xS$ structure, the Ga—Mn bonds were all parallel. However, one-half the In—Mn bonds in the $In_{1-x}Mn_xS$ structure are parallel, but the other one-half are at an angle of 70°. The agreement between theory and experiment presented here is consistent with Mn^{+3} ions going in at the In lattice site.

ACKNOWLEDGMENTS

This work was supported by UNF Research Grants, Donors of the American Chemical Society Petroleum Research Fund PRF No. 40209-B5M, a Purdue University Academic Reinvestment Program, and by the National Science Foundation Grants Nos. DMR-03-05653, DMR-04-05082, and DMR-01-02699.

[1] S.-R. Eric Yang, Jairo Sinova, T. Jungwirth, Y. P. Shim, and A. H. MacDonald, Phys. Rev. B **67**, 045205 (2003).
[2] Manish Jain, Leeor Kronik, James R. Chelikowsky, and Vitaliy V. Godlevsky, Phys. Rev. B **64**, 245205 (2001).
[3] C. Timm and A. H. MacDonald, Phys. Rev. B **71**, 155206 (2005).
[4] S. Hilbert and W. Nolting, Phys. Rev. B **71**, 113204 (2005).
[5] Mark van Schilfgaarde and O. N. Mryasov, Phys. Rev. B **63**, 233205 (2001).
[6] Xuan Luo and Richard M. Martin, Phys. Rev. B **72**, 035212 (2005).
[7] S. Das Sarma, E. H. Hwang, and A. Kaminski, Phys. Rev. B **67**, 155201 (2003).
[8] V. F. Sapega, M. Moreno, M. Ramsteiner, L. Daweritz, and K. Ploog, Phys. Rev. B **66**, 075217 (2002).
[9] H. Saito, V. Zayets, S. Yamagata, and K. Ando, Phys. Rev. B **66**, 081201(R) (2002).
[10] T. M. Schuler, R. A. Stern, R. McNorton, S. D. Willoughby, J. M. MacLaren, D. L. Ederer, V. Perez-Dieste, F. J. Himpsel, S. A. Lopez-Rivera, and T. A. Callcott, Phys. Rev. B **72**, 045211 (2005).
[11] S. Tsoi, I. Miotkowski, S. Rodriguez, A. K. Ramdas, H. Alawadhi, and T. M. Pekarek, Phys. Rev. B **69**, 035209 (2004).
[12] C. Fuller, A. Douglas, J. Garner, T. M. Pekarek, I. Miotkowski, and A. K. Ramdas, Phys. Rev. B **65**, 195211 (2002).
[13] T. M. Pekarek, B. C. Crooker, I. Miotkowski, and A. K. Ramdas, J. Appl. Phys. **83**, 6557 (1998).
[14] T. M. Pekarek, M. Duffy, J. Garner, B. C. Crooker, I. Miotkowski, and A. K. Ramdas, J. Appl. Phys. **87**, 6448 (2000).
[15] T. M. Pekarek, C. Maymi, J. Garner, D. Hall, I. Miotkowski, and A. K. Ramdas, J. Appl. Phys. **91**, 7496 (2002).
[16] T. M. Pekarek, C. L. Fuller, J. Garner, B. C. Crooker, I. Miotkowski, and A. K. Ramdas, J. Appl. Phys. **89**, 7030 (2001).
[17] S. Nusse, P. H. Bolivar, H. Kurz, F. Levy, A. Chevy, and O. Lang, Phys. Rev. B **55**, 4620 (1997).
[18] S. Lee, S. Hahn, C. Chung, S. Yun, and W. Kim, Solid State Commun. **60**, 453 (1986).
[19] K. Watanabe, K. Uchida, and N. Miura, Phys. Rev. B **68**, 155312 (2003).
[20] M. O. D. Camara, A. Mauger, and I. Devos, Phys. Rev. B **65**, 125206 (2002).
[21] F. J. Manion, A. Segura, V. Munoz-Sanjose, G. Tobias, P. Ordejon, and E. Canadell, Phys. Rev. B **70**, 125201 (2004).
[22] C. Julien, M. Eddrief, M. Balkanski, and A. Chevy, Phys. Rev. B **46**, 2435 (1992).
[23] N. C. Fernelius, Prog. Cryst. Growth Charact. Mater. **28**, 275 (1994). The InS structure is also available at the site, www.webelements.com
[24] G. Franzese, Ashlee Byrd, J. L. Tracy, J. Garner, T. M. Pekarek, I. Miotkowski, and A. K. Ramdas, J. Appl. Phys. **97**, 10D308 (2005). This paper presents some magnetization data for $In_{1-x}Mn_xS$ with a brief comparison to the singlet model. For $In_{1-x}Mn_xSe$, see T. M. Pekarek, D. J. Arenas, I. Miotkowski, and A. K. Ramdas, J. Appl. Phys. **97**, 10M106 (2005).
[25] For a review of recent advances of crystal (ligand) field theory, see, for example, *Ligand Field Theory and Its Applications*, edited by B. N. Figgis and M. A. Hitchman (Wiley-VCH, New York, 2000).
[26] S. Jandl, J. L. Brebner, and B. M. Powel, Phys. Rev. B **13**, 686

(1976). See also, M. Schluter and M. L. Cohen, *ibid.* **14**, 424 (1976).

[27] *Progress in Crystal Growth and Characterization of Materials*, edited by J. B. Mullin (Pergamon, New York, 1994), p. 276.

[28] *Electron Paramagnetic Resonance of Transition Ions*, edited by A. Abragam and B. B. Bleaney (Oxford University Press, New York, 1971).

[29] D. Scalbert, J. Cernogora, A. Mauger, C. Benoit à la Guillamine, and A. Mycielski, Solid State Commun. **69**, 453 (1989).

[30] J. P. Mahoney, Chun C. Lin, William H. Brumage, and Franklin Dorman, J. Chem. Phys. **53**, 4286 (1970).

[31] Y. Shapira, J. Appl. Phys. **67**, 5090 (1990).

[32] P. M. Shand, A. D. Christianson, T. M. Pekarek, L. S. Martinson, J. W. Schweitzer, I. Miotkowski, and B. C. Crooker, Phys. Rev. B **58**, 12876 (1998).